International Journal of Thermal Sciences 48 (2009) 1151–1160

Contents lists available at ScienceDirect

International Journal of Thermal Sciences

www.elsevier.com/locate/ijts

Optimization of embedded inclined open-ended channel in natural convection used as heat drain

Yohann Chataigner [a], Louis Gosselin [a,*], Guy Doré [b]

[a] Département de génie mécanique, Université Laval, Québec City, Québec, G1V 0A6, Canada
[b] Département de génie civil, Université Laval, Québec City, Québec, G1V 0A6, Canada

ARTICLE INFO

Article history:
Received 23 July 2008
Received in revised form 19 December 2008
Accepted 2 January 2009
Available online 31 January 2009

Keywords:
Natural convection
Heat drain
Embedded channel
Inclined channel
Chimney
Permafrost
Thawing

ABSTRACT

The heat transfer and self-driven fluid flow within an inclined open-ended channel is presented. The channel is assumed thin and is embedded into a solid. The application that we consider is for the cooling of permafrost on which an infrastructure such as a road is built. A CFD model and a scale analysis are developed. Optimization of the channel is performed by varying its thickness, inclination angle, and entrance length. The overall thermal conductance between air and ground is provided. Based on an equivalent thermal circuit of the inclined channel, transient simulations of the ground are performed in order to verify whether the heat drain helps to elevate the maximal thawing interface during the year. For the case considered, the front moved upwards by more than 30 cm with the heat drain. The model and results could be applied to several other types of embedded open-ended inclined channels.

© 2009 Elsevier Masson SAS. All rights reserved.

1. Introduction

The undergoing global warming is currently jeopardizing permafrost stability in cold regions, and consequently the infrastructures that are built on it. This situation is forcing engineers to propose technological solutions for maintaining the soil below the freezing point. As most permafrost soils contain large amount of frozen water, thawing results in collapsing and destruction of the infrastructures that are built on it. In particular, road infrastructures installed on the permafrost are at stake and efforts are deployed to ensure their integrity. According to a recent official report of the Canadian government on the impacts and adaptations to changing climate [1], Canadians devote 150 billions of dollars to transportation yearly. This demonstrates the importance of transportation and in particular, the challenge of preserving the transport infrastructures in good conditions. Even southward, winter recreational infrastructures such as ice rinks and skiing pathways could also benefit from colder soil for extending their periods of utilization or diminishing their cost of operation.

Several technological solutions have been tested in the last decade for providing additional heat removal from permafrost. Among the most studied technological solutions are the convective embankment – which is a layer or a pile of stones in which Bénard convection and/or wind can enhance heat transfer from the ground to the air [2–8], and the duct-ventilated embankment [9, 10] that rely on wind for cooling the soil. Reflective surfaces have also been studied to diminish the amount of radiation absorbed by the road [11]. These techniques, and others [12], have been documented, tested and modeled over the last decades in order to facilitate the construction of infrastructures on permafrost.

Another solution is a thermal drain installed in the embankment allowing outside cold air to flow in an internal chimney-like channel (natural convection) and thus, to extract more heat from the ground [8]. The heat drain concept – the object of this study – is relatively recent, and therefore, it has been scarcely documented in literature.

In fact, open-ended channels with self-driven flow that have attracted attention were mainly oriented vertically. For example, Bejan showed the potential to maximize the heat transfer rate density of a series of vertical channels: when the channels are thin, fluid flow is blocked, while too large channels are detrimental for compactness [13]. Da Silva et al. have recently maximized the heat transfer density in vertical channels, which walls could rotate symmetrically to create trapezoidal-shaped channels [14] or with optimized distribution of heat sources on its walls [15]. The geometry of C and L-shaped channels was optimized in [16] under natural convection conditions. Optimal inlet and outlet breadths were found to maximize the overall heat transfer rate. In [17], heat transfer is enhanced in vertical plate channel with the insertion of an auxiliary plate and the appendage of two insulated plate extensions. Lakkis and F. Moukalled [18] studied numerically

* Corresponding author. Tel.: +1 418 656 7829; fax: +1 418 656 7415.
E-mail address: Louis.Gosselin@gmc.ulaval.ca (L. Gosselin).

1290-0729/$ – see front matter © 2009 Elsevier Masson SAS. All rights reserved.
doi:10.1016/j.ijthermalsci.2009.01.001

Nomenclature

c_p	heat capacity ..... J/kg K	u, v	velocity components ..... m/s
D	heat drain thickness ..... m	x, y	Cartesian coordinates ..... m
g	gravitational constant ..... m/s^2	z	thickness ..... m
h	convection coefficient ..... W/m^2 K	*Greek symbols*	
k	thermal conductivity ..... W/m K	α	angle ..... °
$\dot{m}$	mass flow rate ..... kg/s	β	thermal expansion coefficient ..... K^{-1}
Nu	Nusselt number	λ	latent heat of melting ..... J/kg
p	pressure ..... N/m^2	μ	dynamic viscosity ..... N s/m^2
q''	heat flux ..... W/m^2	ρ	density ..... kg/m^3
Re	Reynolds number	ν	kinematic viscosity ..... m^2/s
t	time ..... s	ξ, η	coordinates ..... m
T	temperature ..... K		

natural convection flow in channels with a curved wall. The wall shape affected significantly the heat and fluid features of the system. Enhancement of heat transfer removal was lager for larger curvatures and smaller Grashof numbers. Yucel et al. [19], Choi and Ortega [20] and Barletta and Zanchini [21] simulated inclined channels numerically, but under mixed convection conditions and for channel with relatively large breadth. Experimental results and correlations for self-driven flows in such channels are presented in [22]. An important outcome of all the studies on self-driven heat and fluid flow within open-ended channels is the importance of the competition between friction losses (and compactness) versus heat transfer that is taking place when designing such a system, and the optimal tradeoff that has to be made.

In this paper, we study analytically and numerically a thin inclined open-ended channel such as that considered for protecting infrastructures built on permafrost (heat drain concept). By natural convection, air can flow in the heat drain to remove heat from the ground during winter. The objectives of the paper are: (i) to provide a model for assessing the effect of the main geometrical features of the heat drain on its overall performance, (ii) to propose an optimized heat drain design, (iii) to verify the ability of a heat drain to adequately remove heat from the soil. Scale analysis and Computational Fluid Dynamics (CFD) are considered for achieving these objectives. The results presented in this paper could easily be extended other types of heat drains (inclined open-ended channels with self-driven flow) when the objective is to provide better heat extraction.

2. Description of the infrastructure

The embankment considered in the present study is schematized in Fig. 1a. Such a structure is typically found as a shoulder (berm) at the side of roads. Thermally speaking, it constitutes the weakest point of the road design, because contrarily to the road itself it is insulated by the snow during winter (snow is pushed from the road to the shoulder), preventing wintertime cooling. Moreover, the outer surface of the embankment being covered with gravel or sand absorbs summer solar radiation much more than the moss on natural ground. Observations have shown that the berm is where degradations of roads are more likely to happen [23]. Therefore, we focus in this paper on this segment of a road infrastructure, first by considering winter conditions.

The standard embankment considered here is made of material with $k = 1.98$ W/m K. A drain can be placed within the embankment to enhance heat removal from the ground. It consists of a thin air channel, made of flexible plastic and geotextile that can be embedded within the sand. The thermal benefit from the drain stems from buoyancy forces that trigger air flow in the winter. In practice, a buried horizontal pipe is connected to the upper drain

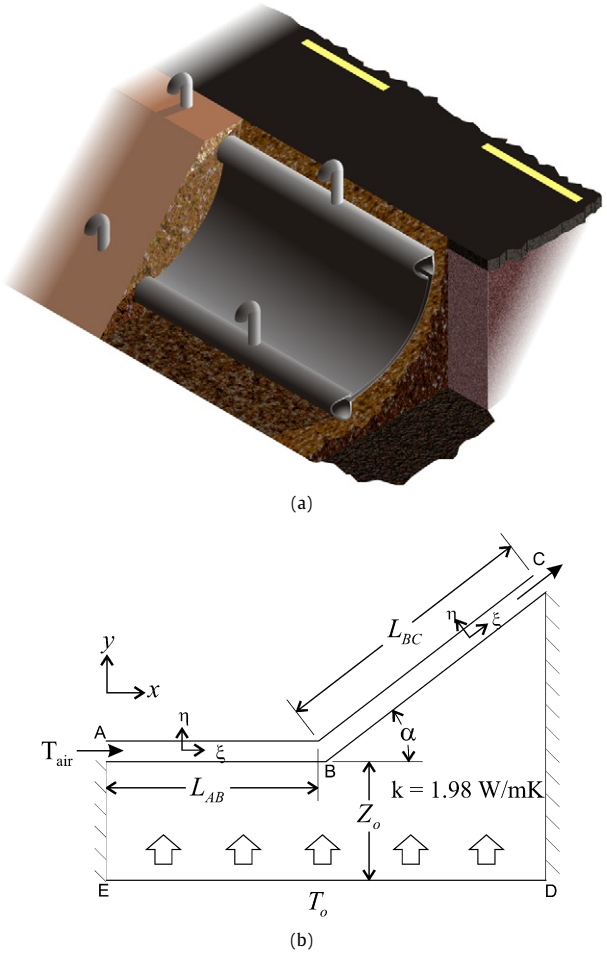

Fig. 1. Schematic representation of the embankment considered in the present study.

opening to collect the air flow and lead it to an external chimney. Similar piping can be installed at the lower drain opening. Nevertheless, a 2D modeling was retained for simplicity (Fig. 1b). On this figure, the section of the berm above the drain has been removed to simplify the problem. Previous results have shown that the presence of this section had a negligible effect on the heat removal during the winter (the temperature is nearly constant and uniform in that zone) [24]. In other words, during the winter, the flow of cold air within the heat drain is assumed to be the dominant heat removal mechanism.

During the winter, the air enters from point A and exits by point C due to buoyancy forces. In practice, the bottom of Fig. 1b

would be in contact with the natural soil (from which heat is flowing in the winter), and the boundary at the point C touches the road. Boundaries AB and CD are in contact with the sand of the embankment.

In the standard embankment material, no flow prevails, and therefore only the conduction equation needs to be solved:

$$\frac{\partial T}{\partial t} = \alpha_{\text{sand}}\left(\frac{\partial^2 T}{\partial x^2} + \frac{\partial^2 T}{\partial y^2}\right) \tag{1}$$

However, in the heat drain itself, temperature gradients induce air density variations and trigger natural convection. Assuming constant properties, Newtonian fluid and laminar flow regime, and applying Boussinesq approximation, the conservation of mass, x-momentum, y-momentum and energy in the heat drain read as (Bejan, 2004 [13]):

$$\frac{\partial u}{\partial x} + \frac{\partial v}{\partial y} = 0 \tag{2}$$

$$u\frac{\partial u}{\partial x} + v\frac{\partial u}{\partial y} = -\frac{1}{\rho}\frac{\partial p}{\partial x} + \nu\left(\frac{\partial^2 u}{\partial x^2} + \frac{\partial^2 u}{\partial y^2}\right) \tag{3}$$

$$u\frac{\partial v}{\partial x} + v\frac{\partial v}{\partial y} = -\frac{1}{\rho}\frac{\partial p}{\partial y} + \nu\left(\frac{\partial^2 v}{\partial x^2} + \frac{\partial^2 v}{\partial y^2}\right) - g\beta(T - T_{\text{ref}}) \tag{4}$$

$$u\frac{\partial T}{\partial x} + v\frac{\partial T}{\partial y} = \alpha\left(\frac{\partial^2 T}{\partial x^2} + \frac{\partial^2 T}{\partial y^2}\right) \tag{5}$$

The variables are defined in the nomenclature. No slip, and temperature and heat flux continuity are imposed on boundaries of the heat drain. The pressure (without the hydrostatic pressure) is set to zero at points A and C in such a way that the flow is solely caused by natural convection. Boundaries AB, BC, CD and AE of Fig. 1b are considered adiabatic. Finally, a fixed temperature was imposed at the bottom of Fig. 1b. Note that the ground and air temperatures will evolve in time due to the weather conditions. This will be discussed later in the paper. The figure of merit is the heat transfer rate removed from the bottom. The different designs considered will be compared on the basis of this criterion.

3. Scale analysis

In this section, we present a scale analysis in order to predict the overall behavior of the heat drain and to determine the most influential parameters. The CFD results will be confronted to the prediction of the scale analysis in Sections 5 and 6. The objective of the scale analysis is to provide a simplified, easy-to-use and fast model for assessing the impact of the main parameters of the heat drain on its thermal performance. For the analysis, a reference coordinate system is introduced with the ξ-axis parallel to the drain, and the η-axis, perpendicular to the drain. Therefore (ξ, η) is equivalent to (x, y) in the flat portion of the drain, but not in the inclined portion. We begin the analysis with a momentum balance in the ξ-direction. We assume that the flow is developed in the drain, which is justified thanks to the fact that the drain is thin and long, yielding $\partial u_\xi/\partial\xi = 0$ and $u_\eta = 0$. Furthermore, we have $\partial^2 u_\xi/\partial\xi^2 \ll \partial^2 u_\xi/\partial\eta^2$ because the thickness of the channel is much smaller than its length. Therefore, $\partial^2 u_\xi/\partial\xi^2$ can be neglected in front of $\partial^2 u_\xi/\partial\eta^2$. Furthermore, the inertial terms are all negligible because the flow is laminar. In the end, the momentum balance in the drain yields

$$-\frac{1}{\rho_{\text{air}}}\frac{\partial p}{\partial \xi} + \nu_{\text{air}}\frac{\partial^2 u_\xi}{\partial \eta^2} - g\beta\big(T_m(\xi) - T_\infty\big)\sin\alpha(\xi) = 0 \tag{6}$$

where $\alpha(\xi)$ is the inclination of the drain with respect to horizontal at the position ξ. In our case, we considered that $\alpha(0 < \xi < L_1) = 0$ and $\alpha(\xi > L_1) = \alpha_0$. T_m is the averaged fluid temperature which varies in the ξ-direction only. Eq. (6) will be integrated from the inlet of the drain to its outlet. Assuming fully developed flow, the velocity profile within the channel is parabolic, $u_\xi = (3\bar{u}_\xi/2)[1 - (2\eta/D)^2]$, and therefore, the central term of Eq. (6) does not vary with ξ, and could be replaced by

$$\nu\frac{\partial^2 u_\xi}{\partial \eta^2} \approx 12\nu\frac{u_\xi}{D^2} \tag{7}$$

Then, we perform the integration of Eq. (6) yielding

$$u_\xi = \frac{g\beta D^2 \sin\alpha_0}{12\nu(L_{AB} + L_{BC})}\int_B^C \big(T_m(\xi) - T_\infty\big)\,d\xi \tag{8}$$

where we have considered $p_C = p_A$ because the drain works solely in natural convection and p here is the total pressure without the hydrostatic pressure. The two unknowns that we want to determine are the velocity u_ξ and temperature T_m. Eq. (8) is a first relation between both unknowns. Note that the self-driven velocity in Eq. (8) adapts to the geometrical features of the channel (i.e., flow resistance), thanks to the second term in Eq. (6) which represents friction forces.

A second equation relating u_ξ and T_m is required, and is built from the conservation of energy principle. At a position ξ, heat is transferred from the ground to the channel and follows two thermal resistance (conduction in the ground layer of thickness $z(\xi)$, and internal convection). Therefore, the energy balance is

$$(\rho c_p)_{\text{air}} u_\xi \frac{dT_m}{d\xi} = \frac{T_0 - T_m}{R''(\xi)} \quad \text{with } R''(\xi) = \frac{z(\xi)}{k_g} + \frac{1}{h} \tag{9}$$

where h is the internal convection coefficient and can be determined from appropriate correlation. For example, for laminar flow, we have $h \sim 5k_{\text{air}}/D$ [7]. Eqs. (8)–(9) forms a set of two equations with two unknowns. We solved them in an order of magnitude sense. We replaced the integral in Eq. (8) by

$$\int_B^C \big(T_m(\xi) - T_\infty\big)\,d\xi \sim \frac{(T_{m,B} + T_{m,C})L_{BC}}{2} \tag{10}$$

and integrated Eq. (9) from A to B, and from B to C.

$$\frac{T_{m,B} - T_0}{T_{m,A} - T_0} = \exp\left(-\frac{L_{AB}}{\bar{R}''_{AB}\rho c u_\xi D}\right) \tag{11}$$

$$\frac{T_{m,C} - T_0}{T_{m,B} - T_0} = \exp\left(-\frac{L_{BC}}{\bar{R}''_{BC}\rho c u_\xi D}\right) \tag{12}$$

where:

$$\bar{R}''_{AB} = \frac{z_0}{k_g} + \frac{1}{h}$$

$$\bar{R}''_{BC} = \left[\frac{1}{L_{BC}}\int_0^{L_{BC}}\left(\frac{z(\xi)}{k_g} + \frac{1}{h}\right)^{-1} d\xi\right]^{-1} \tag{13}$$

In the end the two unknowns (i.e., air velocity and temperature) can be determined from the following set of equations

$$u_\xi = \frac{g\beta D^2 \sin\alpha_0 L_{BC}}{12\nu(L_{AB} + L_{BC})}\left(\frac{T_B + T_C}{2} - T_\infty\right) \tag{14}$$

$$\frac{T_B + T_C}{2} = T_0 + \frac{T_\infty - T_0}{2}\exp\left(-\frac{L_{AB}}{\bar{R}''_{AB}\rho c u_\xi D}\right) \times \exp\left(-\frac{L_{BC}}{\bar{R}''_{BC}\rho c u_\xi D}\right) \tag{15}$$

Even though it is not possible to express the unknowns in a closed form, Eqs. (14)–(15) are easily solvable numerically. It is worth to

mention one more time that these equations allow calculating the heat drain performance in the winter only, under a quasi-steady regime. These simple equations will be compared to the CFD results in Sections 5-7.

4. Presentation of the CFD model

The governing equations (2)–(5) have also been solved with a commercial code (Fluent, 1998 [25]) relying on the finite volume approach. The domain is discretized with a quadrilateral control volumes into the drain and triangular control volumes everywhere else. The governing equations are integrated on each control volume, which after appropriate interpolations yield a set of algebraic equations that can be solved iteratively. Convergence is declared when the residuals have dropped by three orders of magnitude for the momentum and mass conservation equations, and 6 orders of magnitude for the energy equation.

The results have been carefully tested for mesh independence by ensuring that doubling the mesh density resulted in variations of the heat transfer rate removed from the bottom smaller than 1%. The numerical model was validated with lab experimental data (Jørgensen et al., 2007 [8]), in stead-state and with $T_\infty = -17\,^\circ\mathrm{C}$ and $T_{AH} = 0\,^\circ\mathrm{C}$. The numerical model proved to predict temperature in the system within 0.5 °C under the drain and therefore, was judged satisfactory.

5. Effect of the heat drain length

Fig. 2 presents the effect of L_{AB} on the averaged velocity, temperature, and heat transfer removal as calculated by the CFD model while the other parameters are kept constant ($L_{BC} = 10$ m, $\alpha = 45°$, $D = 0.025$ m, $Z_0 = 0.10$ m, $T_{\mathrm{air}} = -35\,^\circ\mathrm{C}$, $T_0 = 0\,^\circ\mathrm{C}$). As expected, longer entrance L_{AB} tends to increase the temperature in the heat drain by increasing the heat transfer surface area. This is beneficial to generate the self-driven flow. On the other hand, longer channel also increases the friction losses and contributes to braking the air flow. This competition between buoyancy and friction explains the presence of a length that maximizes the velocity. In the end, the overall heat transfer removed from the ground was found to increase with L_{AB} for the range tested. However, the improvement in terms of heat transfer removal decreases as L increases (diminishing return).

Also, the outcome of the scale analysis developed in Section 3 is confronted to the CFD results in Fig. 2. The difference of velocity calculated from CFD and that of the scale analysis was less than 10%. Similarly, the temperature difference was less than 0.3 °C for all cases tested. Most importantly, for the figure of merit (heat removal), the maximal discrepancy between the CFD and scale analysis was 15%, and was achieved for smaller L_{AB}-values. The correspondence between the CFD and scale results was considered excellent considering the simplicity of the scale analysis.

6. Effect of the heat drain position within the embankment

An important design consideration is the position of the drain within the embankment. We considered the effect of the angle α on the average velocity, outlet temperature and heat transfer removal, see Fig. 3, while the other parameters are kept constant as in Section 5 (with $L_{AB} = 10$ m). The averaged velocity increases with the inclination angle, due to the enhancement of the buoyancy forces. Accordingly, the outlet temperature tends to decrease with the inclination angle because the air flow is stronger for large angle. In the end, the heat removal was found to be larger for more inclined outlet, but again, diminishing return was observed, i.e. that at some point increasing further the inclination angle will not yield significant improvement. Also it is worth to mention that

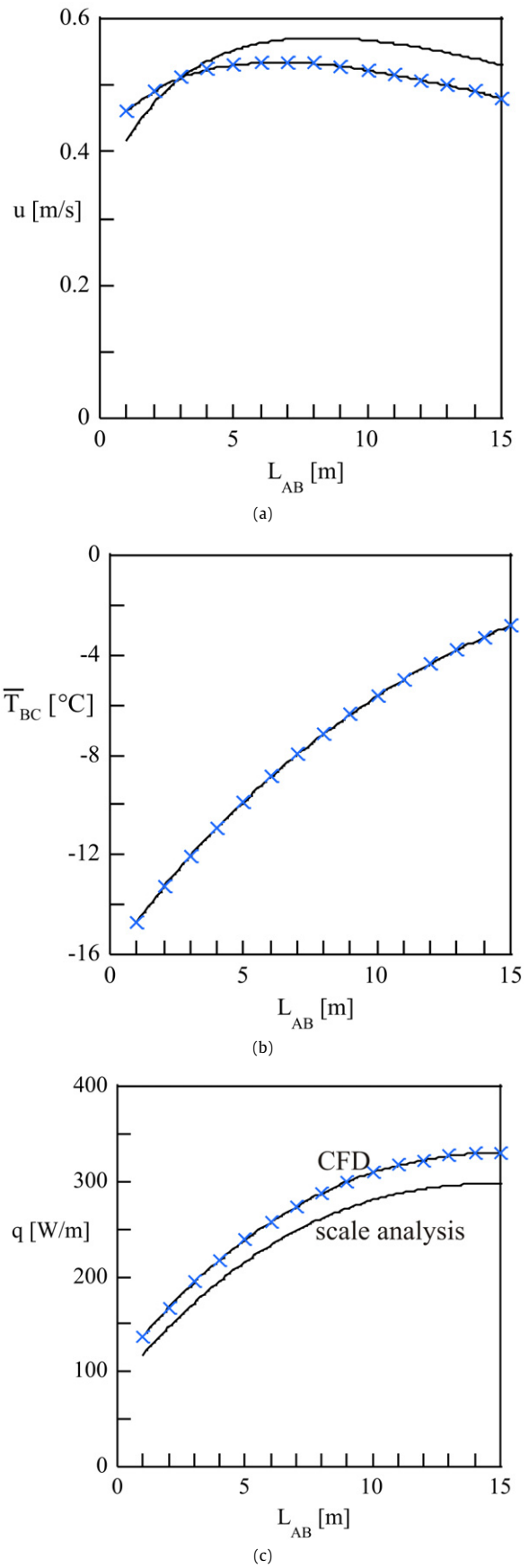

Fig. 2. Effect of the entrance zone length L_{AB} on: (a) average velocity, (b) average outlet temperature, and (c) heat removal from the ground.

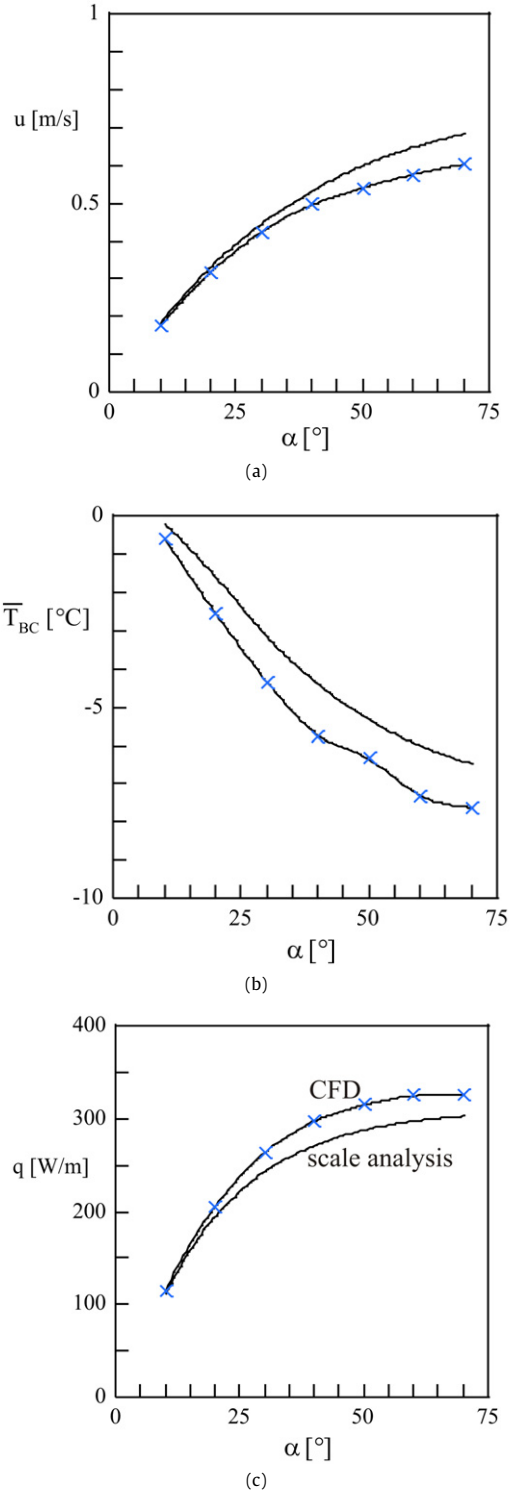

Fig. 3. Effect of the inclination angle α on: (a) average velocity, (b) average outlet temperature, and (c) heat removal from the ground.

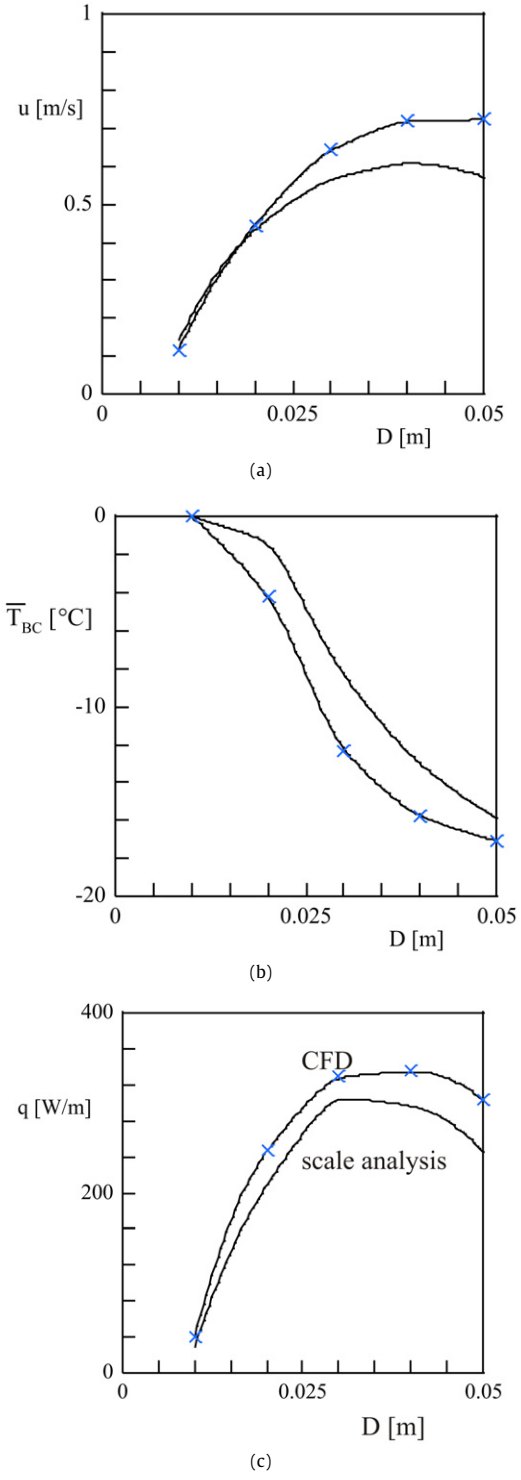

Fig. 4. Effect of the drain thickness D on: (a) average velocity, (b) average outlet temperature, and (c) heat removal from the ground.

large values of inclination are not always feasible in practice, at least for the application envisioned here (road shoulder on permafrost).

Once again, the comparison with the scale analysis results was found to be excellent: the maximal relative error for u was 13% (for larger angle of inclination), the maximal temperature difference was 1.1 °C (also for larger angle of inclination, and the maximal relative error for the heat transfer removal was less than 9%). The fact that the error introduced by the scale analysis model is larger for very inclined channel could be explained by that fact that the flow resistance associated with the knee was not modeled in Section 3. Therefore, the scale analysis will tend to overestimate the velocity especially for very inclined channels.

7. Effect of the heat drain thickness

Another important parameter to consider in the heat drain thickness D. The CFD results are shown in Fig. 4 with an angle $\alpha = 45°$ and an entrance length $L_{AB} = 10$ m. Thicker channel

will facilitate air flow (smaller flow resistance) and at the same time, will reduce the internal heat transfer coefficient (thus impairing air heating and buoyancy). This competition explains the presence of a thickness that maximizes the average velocity. The temperature on the other hand, decreases monotonically with D due to the diminution of the internal heat transfer coefficient. Finally, the overall heat transfer rate exhibit a maximum for which the thickness provides a good trade-off between a good heat transfer coefficient and a small flow resistance. Again, it is worth to mention that the flow resistance influences the self-driven mass flow rate, both with the CFD analysis and with the scale analysis.

Scale analysis results are also shown in Fig. 4, and again compared well with CFD results. In particular, the maximal heat transfer removal is visible from the scale results. The maximal error (27%) was achieved for very thin channel. Even though this relative error may seem larger than that mentioned in the previous sections, it should be pointed out that the absolute error is not large as thin channel led to very small heat transfer removal with both approaches.

8. Design considerations

The results of the scale analysis have proven to yield satisfactory results compared to CFD results, in a much simpler and "practical" way. The error of prediction for the heat transfer removal rate was less than 15% for most of the case considered. For field engineers, the results of Section 3 are easier and faster to use when designing a heat drain system than performing a CFD analysis.

The main design lessons learned from the results presented so far are: (i) longer channels are better, (ii) larger inclination angles are better, (iii) there is an optimal channel thickness. However, these results were achieved by varying one design variable at a time, while keeping the others constant. This is unlikely to provide optimal design and to respect the various constraints that practice engineers face when designing. Therefore, we propose in this section to investigate further the designing process and to propose useful tools for doing so. The figure of merit considered is still the heat removal rate.

For the sake of illustration, we considered throughout this section a shoulder with an on-ground spanning width of 10 m. In other words, the lengths L_{AB} and L_{BC}, and the angle of inclination are not all independent anymore, but are related by the relation: $10\ \mathrm{m} = L_{AB} + L_{BC}\cos\alpha$. This leaves three design variables to fully characterize geometry. We considered here D, α and L_{AB}. The length L_{BC} was calculated from the constraint invoked above. The scale analysis model was put to use. As we have noted above, the thickness D can be optimized for maximizing the heat transfer rate. Therefore, for each set of α and L_{AB}, we varied D until the optimal value was identified, D_{opt}. This optimal drain thickness is reported in Fig. 5a as a function of α and L_{AB}. Thicker drain is required for low inclination heat drains with a long flat entrance zone. Most of the times, the optimal channel thickness was between 2 and 3.5 cm. In Fig. 5b, we reported the maximal heat transfer rate corresponding to the optimal drain thickness shown in Fig. 5a. It is interesting to note that for each inclination angle, there is a value of L_{AB} that also maximizes the heat removal. These values have been reported in Fig. 6 as a function of the angle α. The best value of L_{AB} to consider should thus be related to the choice of α in the designing process. In the end, our results showed that larger values of α led to more heat removal (Fig. 6b). However, practical reasons might prevent the inclination angle from being too large. During the installation, the ground under the channel will first be prepared, and then the channel will be sited on it before being covered with more sand. It is unlikely that very steep shapes will hold easily before the drain is installed. Inclination angle larger than $\sim 45^\circ$ would be costly and technically difficult to consider. Therefore, for the conditions considered here, the optimal channel would have $\alpha \sim 45^\circ$, and its entrance flat length and thickness would be chosen from Figs. 6a and 6b respectively for that angle.

9. Transient simulations

Real heat drains work under transient regime, as outdoor and ground temperatures vary in time. Therefore, one could argue that the present steady-state approach is not applicable, and that the choice of temperature T_0 and T_∞ is arbitrary. To address this point, it is useful to draw a parallel between the design of the heat drain and the design of a building heating system. When designing a building heating system, for simplicity, the "design heat load" could be calculated based on steady-state calculations and using indoor and outdoor "design temperatures" [26]. It is understood that the heating system will not always work at the design heat load and temperatures, but the calculation aims at sizing and (pre-)designing a robust heating system. After the dimensioning, energy simulation could be performed to establish the detailed building transient behavior. Similarly, in this paper, the model is useful to design the system, but it is clear that a complete picture will be achieved only by considering the transient behavior of the system. Two design temperatures are invoked (i.e., ground and air temperatures). The temperatures chosen in the previous sections were characteristic temperatures of air and ground in winter for cold climates. To illustrate the effect of the design temperatures, the heat drain was optimized with $\alpha = 45^\circ$ (i.e., larger angle achievable) for different values of the design temperature difference, $T_\infty - T_0$. The optimal thickness and heat drain entrance length are shown in Fig. 7a. These optimal design parameters are relatively insensible to the design temperature difference. This robustness is useful from a design perspective. Fig. 7b shows the heat transfer rate as a function of the temperature difference. The performance of the heat drain is obviously affected by the design temperature difference even though the optimal design remains almost the same. A nearly linear relationship is observed between the heat removal and the design temperature difference. The slope of the fitting curve is 11.257 W/m K ($R^2 = 0.9868$) which corresponds to a thermal resistance of 0.0888 K m/W. Considering the span of the system (10 m), the thermal resistance is estimated to 0.888 K m^2/W for the system considered so far. This thermal resistance connects the natural ground surface to the exterior air. In the absence of drain, the thermal resistance would have been dominated by conduction in the sand and in the snow cover. Assuming (in addition to the sand below the drain) a 30 cm cover of sand (k varying between 0.5 and 2 W/m K) and a 30 cm of snow (k varying between 0.05–0.2 W/m K), we estimated the winter thermal resistance in the absence of heat drain to vary between 1.7 and 6.8 K m^2/W. We assumed an average value of the winter thermal resistance without the heat drain for the simulations presented below, i.e., 4.25 K m^2/W. In any case, the heat drain decreases by a significant factor the overall thermal resistance of the shoulder. In other words, the heat drain enhances heat evacuation from the ground during winter.

In the summer, the ground is colder than air, and therefore, there is no flow within the heat drain. The summer thermal resistance of the shoulder is estimated to 0.4 K m^2/W, i.e. smaller than the winter thermal resistance without heat drain (because of the absence of snow cover) but larger than the winter thermal resistance with the heat drain. In the summer, the heat drain (when present) would represent a thin air layer that acts as an insulator and increases the resistance by 0.08 K W/m^2. Larger thermal resistance in the summer is beneficial because is prevents heat from penetrating in the ground. Fig. 8 shows a thermal representation of

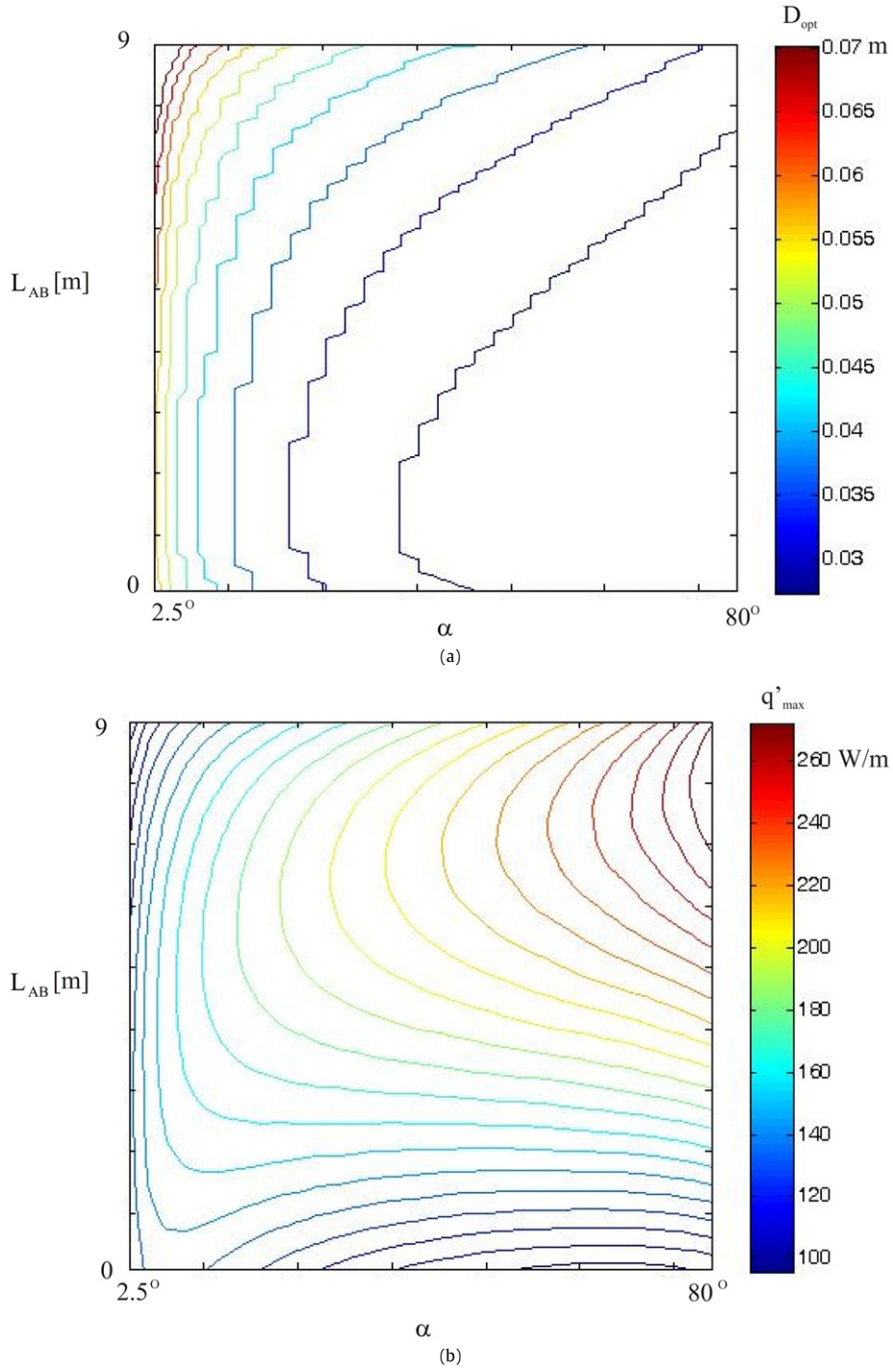

Fig. 5. (a) Optimal drain thickness and (b) maximal heat transfer rate removal as a function of L_{AB} and α.

the shoulder with the heat drain in which the thermal inertia of the shoulder is neglected. When $T_\infty > T_0$ (summer), heat flows in the right-hand branch of the circuit, and when $T_\infty < T_0$ (winter), heat flows in the left-hand side branch. The drain could thus be envisioned as a circuit involving thermal diodes that prevent heat from penetrating in the ground in the summer and enhance heat evacuation in the winter, because $R''_{\text{winter}} < R''_{\text{summer}}$. Such a circuit could be used in transient simulations. For example, it could be added to other thermal resistances and capacitances such as that of natural ground below the shoulder to simulate the whole behavior of the system. It could also serve to determine the boundary conditions at the surface of natural ground in a numerical finite-volume or finite-element model. In any case, the value of the resistance R''_{winter} when the heat drain is active can be determined from the model developed in this paper for the heat drain geometry desired.

A simulation has been performed with a 1D ground model and the thermal circuit of Fig. 8 to determine the ground surface boundary condition. The ground model relies on finite volumes and includes the phase change. Mesh and time step independence were verified. The properties considered for the ground were $k = 1.438$ W/m K, $\rho c_p = 2118$ kJ/m^3 K, $\lambda = 50.2$ kJ/kg and for air $k = 0.025$ W/m K, $\rho c_p = 1.1717$ kJ/m^3 K and $\mu = 1.596 \times 10^{-5}$ N s/m^2. The idealized air temperature considered followed a sinusoidal: $T_{\text{air}}(t) = [-5 + 20\sin(\omega t)]\,^\circ$C where ω is the angular frequency

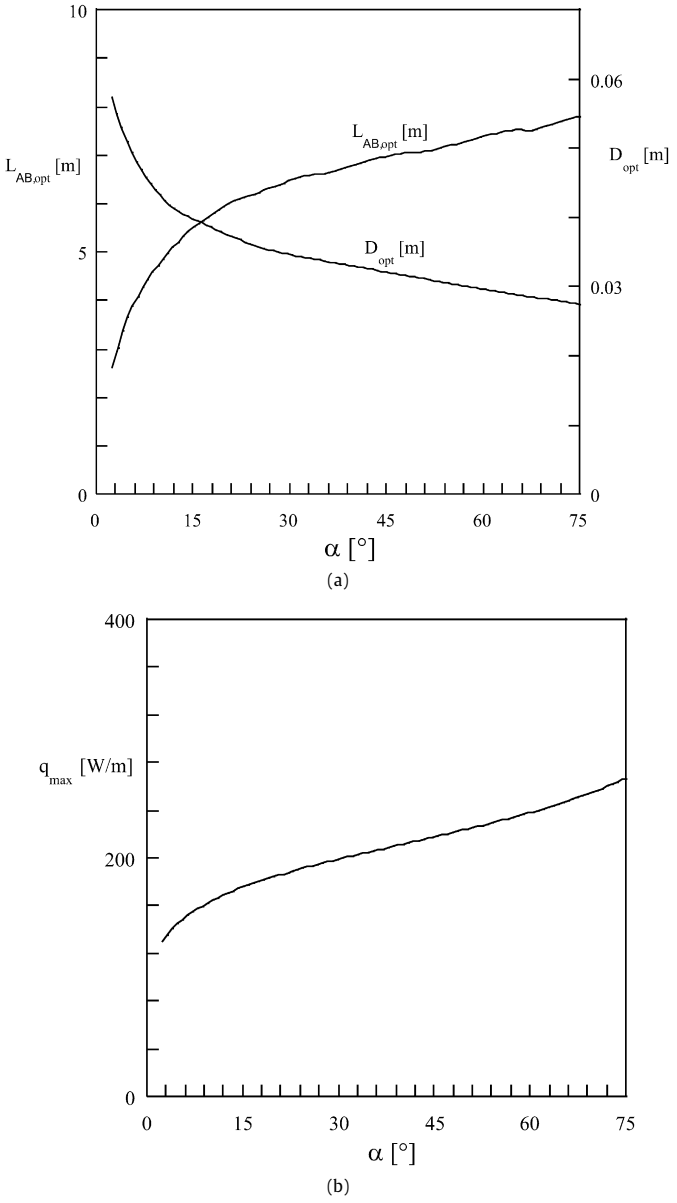

Fig. 6. Optimal drain thickness, entrance length and maximized heat transfer removal as a function of the angle α.

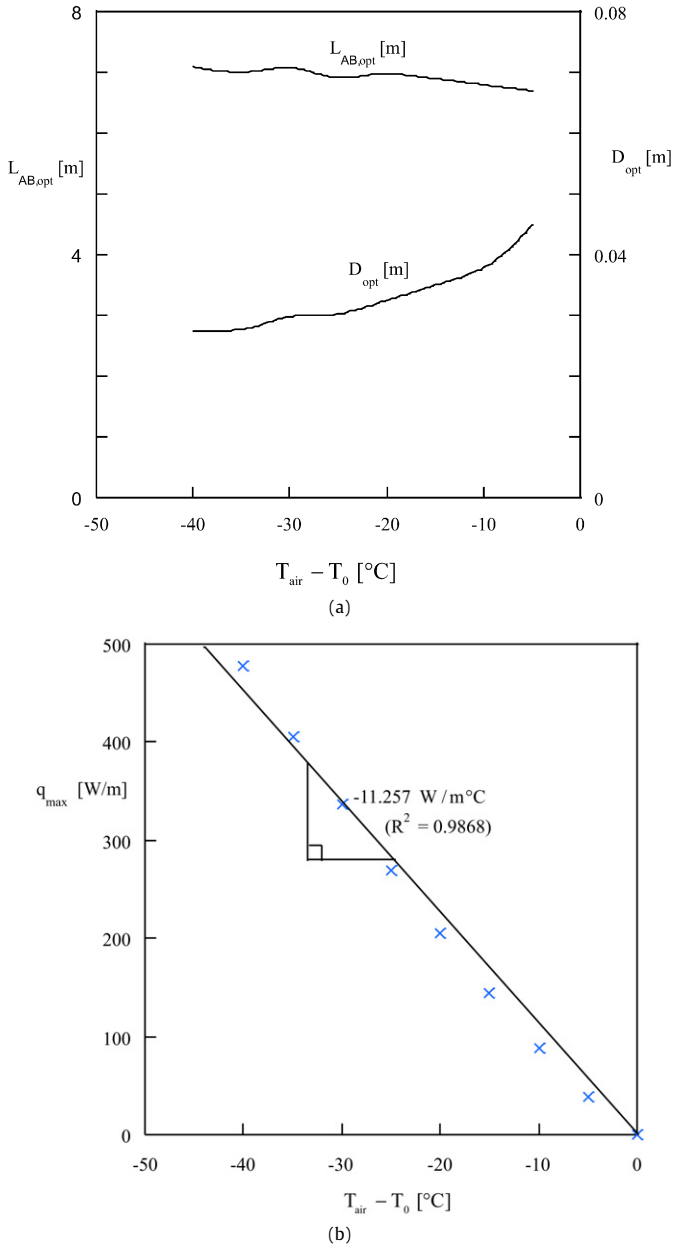

Fig. 7. Effect of the design temperature difference on (a) the optimal parameters and (b) maximized heat transfer removal rate.

corresponding to 1 year. The height of ground considered was 15 m and the deep ground temperature was kept at −5 °C. These typical values of temperatures were retained based on experimental measurements [27]. The periodic regime was determined (i.e., the yearly simulation is repeated over and over, until the temperature profile repeats exactly every year) and is shown in Fig. 9 with and without the heat drain. The effect of the heat drain is to facilitate the evacuation of heat thus creating a larger pocket of cold in the ground that helps containing the heat penetration in the summer. Overall, the heat drain allowed elevating the maximal melting front and reducing ground temperature. Even though this 1D model is simplistic, it yields satisfactory results (the results are coherent with more complex modeling of the heat drain [8,24]) and is helpful and quick in a pre-design phase. This model is not intended to provide a detailed 2D or 3D transient temperature profile but rather to determine roughly the shoulder's main features required to elevate the active soil layer as high as required. This model could eventually be validated with in situ measurements, but it is important to recall that such measurements are difficult and expensive to perform not only due to the cold climate, but also

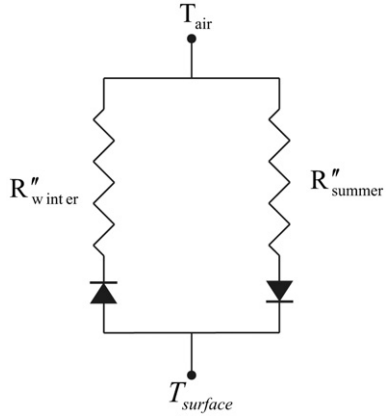

Fig. 8. Equivalent thermal circuit of the shoulder with heat drain.

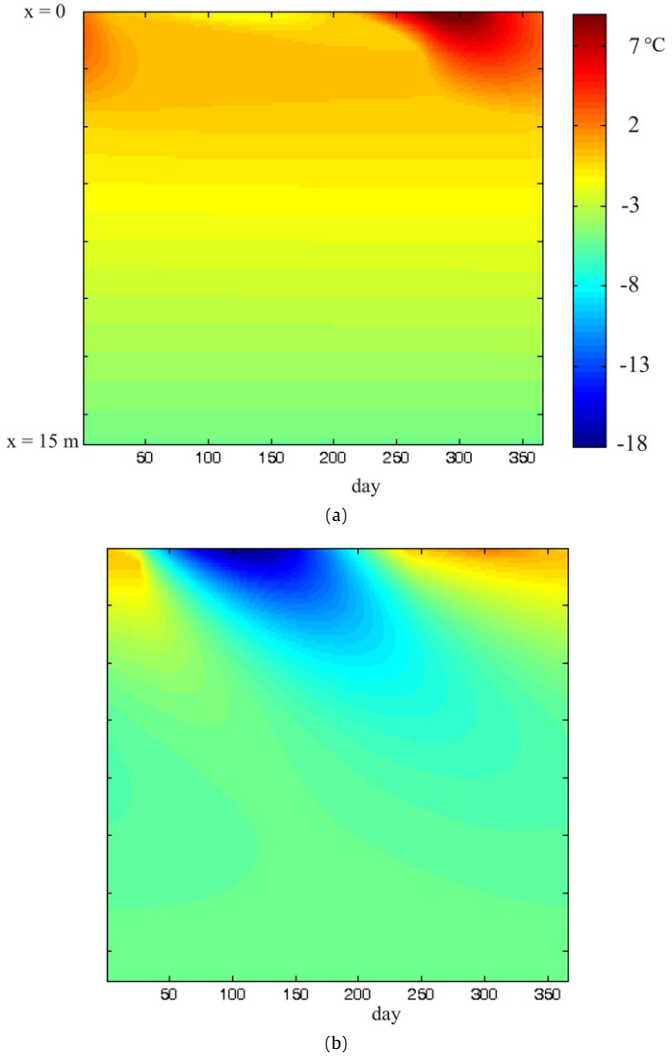

Fig. 9. The temperature profile in the ground as a function of time (a) without the heat drain, and (b) with the heat drain.

due to the remoteness and small population of the regions with permafrost (e.g., Nunavik (Northern region of the Québec Province) has a population of ∼11,000 with a surface area larger than California, and the main village, Kuujjuaq, is ∼1300 km from Quebec City). This emphasizes one more time the importance of designing good infrastructures and the usefulness of numerical tools in doing so. Further work could simulate with the coarse model presented in this paper several different types of ground and weather conditions to assess the efficiency of the heat drain for permafrost protection.

10. Conclusions

We proposed a simple model based on scale analysis and validated with CFD to evaluate the performance of a heat drain which consists of an inclined and embedded open-ended channel. Such a heat drain is envisioned for permafrost protection in cold regions but the model and concepts presented in the paper could be applied to other applications.

The geometry of the channel (e.g., length, angle of inclination, thickness) has been optimized for maximizing its cooling effect. We found that more inclined channels worked better, and that the optimal flat entrance length increased with α while the optimal diameter diminished. For a fixed angle of inclination, the optimal design was relatively insensible to the design temperature difference (robustness). The heat removed by the optimal design was proportional to the design temperature difference, which allowed us to determine an equivalent thermal resistance for the system connecting the exterior air temperature to the surface of the natural ground. In the end, an equivalent thermal circuit is proposed to represent the connection between the air and the ground surface. This thermal circuit is used to simulate the thermal transient behavior of the ground over the year.

The elements proposed in this paper constitute useful tools from a design point-of-view. In particular, they are easy to use for heat transfer non-specialists. The exploitation of the model to build abacuses directly usable by designers will be a future continuation of this work. Results could be extended to other heat removal systems relying on natural convection. Further research could focus on other channel shapes as well as other applications. In some cases, networks of channels could also be envisioned in relation with the idea of designed porous media for natural convection cooling (see, e.g., [13,28]) in which several cooling channels are organized to work together for maximal overall system performance.

Acknowledgements

L. Gosselin's work was supported by the Natural Sciences and Engineering Research Council (NSERC) of Canada.

References

[1] F.J. Warren, et al., Climate Change Impacts and Adaptation: A Canadian Perspective, Natural Resources Canada, Government of Canada, 2004, pp. 145–159. http://adaptation.nrcan.gc.ca/perspective/index_e.php.
[2] M.Y. Zhang, Y.M. Lai, Z.Q. Liu, Z.H. Gao, Nonlinear analysis for the cooling effect of Qinghai-Tibetan railway embankment with different structures in permafrost regions, Cold Regions Science and Technology 42 (3) (2005) 237–249.
[3] M.Y. Zhang, Y.M. Lai, W.B. Yu, Z.J. Huang, Experimental study on influence of particle size on cooling effect of crushed-rock layer under closed and open tops, Cold Regions Science and Technology 48 (3) (2007) 232–238.
[4] G.Y. Li, N. Li, J.M. Kang, Preliminary study on cooling effect mechanisms of Qinghai-Tibet railway embankment with open crushed-stone side slope in permafrost regions, Cold Regions Science and Technology 45 (3) (2006) 193–201.
[5] W.B. Yu, Y.M. Lai, X.F. Zhang, et al., Laboratory investigation on cooling effect of coarse rock layer and fine rock layer in permafrost regions, Cold Regions Science and Technology 38 (1) (2004) 31–42.
[6] D.J. Goering, Passively cooled railway embankments for use in permafrost areas, Journal of Cold Regions Engineering 17 (3) (2003) 119–133.
[7] D.J. Goering, P. Kumar, Winter-time convection in open-graded embankments, Cold Regions Science and Technology 24 (1) (1996) 57–74.
[8] A.S. Jørgensen, G. Doré, É. Voyer, Y. Chataigner, L. Gosselin, Optimization of the characteristics of two heat removal techniques for permafrost protection, Cold Regions Science and Technology 53 (2) (2008) 179–192.
[9] M.Y. Zhang, Y. Lai, F. Niu, S. He, A numerical model of he coupled heat transfer for duct-ventilated embankment under wind action in cold regions and its application, Cold Regions Science and Technology 45 (2) (2006) 103–113.
[10] F.J. Niu, G.D. Cheng, H.M. Xia, L.F. Ma, Field experiment study on effects of duct-ventilated railway embankment on protecting the underlying permafrost, Cold Regions Science and Technology 45 (3) (2006) 178–192.
[11] Chenji, Huzeyong, Doushun, Qianzeyu, Yin-Yang, Slope problem along Qinghai-Tibetan Lines and its radiation mechanism, Cold Regions Science and Technology 44 (3) (2006) 217–224.
[12] A.L. Evans, R.L. Reid, Heat transfer in an air thermosyphon permafrost protection device, Journal of Energy Resources Technology – Transactions of the ASME 104 (3) (1982) 205–210.
[13] A. Bejan, Convection Heat Transfer, 3rd ed., Wiley, 2004.
[14] A.K. Da Silva, A. Bejan, S. Lorente, Maximal heat transfer density in vertical morphing channels with natural convection, Numerical Heat Transfer Part A – Applications 45 (2) (2004) 135–152.
[15] A.K. da Silva, G. Lorenzini, A. Bejan, Distribution of heat sources in vertical open channels with natural convection, International Journal of Heat and Mass Transfer 48 (2005) 1462–1469.
[16] A.K. da Silva, L. Gosselin, Optimal geometry of L and C-shaped channels with maximum heat transfer rate in natural convection, International Journal of Heat and Mass Transfer 48 (3–4) (2005) 609–620.
[17] A. Andreozzi, A. Campo, O. Mancam, Compounded natural convection enhancement in a vertical parallel-plate channel, International Journal of Thermal Sciences 47 (2008) 742–748.

[18] I. Lakkis, F. Moukalled, Natural-convection heat transfer in channels with isothermally heated convex surfaces, Numerical Heat Transfer Part A 53 (2008) 1176–1194.
[19] C. Yucel, M. Hasnaoui, L. Robillard, E. Bilgen, Mixed convection heat-transfer in open-ended inclined channels with discrete isothermal heating, Numerical Heat Transfer Part A – Applications 24 (1) (1993) 109–126.
[20] C.Y. Choi, A. Ortega, Mixed convection in an inclined channel with a discrete heat source, International Journal of Heat and Mass Transfer 36 (12) (1993) 3119–3134.
[21] A. Barletta, E. Zanchini, Time-periodic mixed convection in an inclined channel, International Journal of Heat and Mass Transfer 45 (2003) 551–563.
[22] O. Manca, S. Nardini, V. Naso, Effect on natural convection of the distance between an inclined discretely heated plate and a parallel shroud below, Journal of Heat Transfer – Transactions of the ASME 124 (3) (2002) 441–451.
[23] G. Doré, I. Beaulac, Y. Shur, Performance of the Alaska Highway in the Beaver Creek Area, Research report, Civil Engineering Department, Université Laval University, pp. 87–90.
[24] Y. Chataigner, Modélisation du transfert thermique dans un remblai sur pergélisol et élaboration de stratégies pour faire face aux changements climatiques, Master's Dissertation, Université Laval, 2008, pp. 61–62.
[25] Fluent 6.3.26, Fluent User's Guide, Fluent Incorporated, 1998, www.fluent.com.
[26] F.C. McQuiston, J.D. Parker, J.D. Spitler, Heating, Ventilating, and Air Conditioning, Analysis and Design, 6th ed., Wiley, 2005.
[27] I. Beaulac, A.-M. Langlois, G. Doré, Évaluation préliminaire de la performance des technologies d'adaptation prometteuses par de la modélisation 1D, Rapport GCT-2006-06, Civil Engineering Department, Université Laval (in French).
[28] C. Villemure, L. Gosselin, G. Gendron, Minimizing hot spot temperature of porous stackings in natural convection, International Journal of Heat and Mass Transfer 51 (15–16) (2008) 4025–4037.